Nuclear Science and Techniques (2026) 37:59
https://doi.org/10.1007/s41365-025-01874-2

Generalized reduced R-matrix theoretical analysis of the ^{5}He system

Xu Han[1] · Tao Ye[2] · Zhen-Peng Chen[3] · Hai-Rui Guo[2] · Wei-Li Sun[2] · Zhi-Hao Sun[1] · Hao-Yang Fan[1]

Received: 12 April 2025 / Revised: 29 May 2025 / Accepted: 30 June 2025 / Published online: 28 January 2026

Abstract
Based on the generalized reduced R-matrix theory, the R-matrix analysis code (RAC program) was used to analyze the experimental data of all the nuclear reaction channels related to the ^{5}He system. The current calculations provide accurate and reliable evaluation data and are in good agreement with the experimental data. In this study, self-consistent evaluation data for each reaction were obtained using multi-channel and multi-energy fitting. In particular, the error propagation theory of generalized least squares was used to determine the error of the evaluation data and the covariance matrix of the integral cross section. This R-matrix analysis for the ^{5}He system has three features. First, for the first time, the error in the evaluation data of the T(d,n)^{4}He reaction cross section and the covariance matrix of the integral cross section are provided. Second, we used only one set of R-matrix parameters to depict the reaction cross section of each reaction channel of the ^{5}He system for the entire energy region in our work. Third, in this evaluation, we considered some of the latest measured experimental data, especially after 2000. The T(d,n)^{4}He reaction cross section at 0.1 MeV and below was carefully studied. The effect of different energy levels in T(d,n)^{4}He was analyzed, with the energy levels $3/2^{+}$ making a major contribution to the cross section, and the role of the S-wave and P-wave from $3/2^{-}$ determines the lean forward trend of the angular distributions at 0.01–0.1 MeV.

Keywords R-matrix theory · Nuclear reaction cross section · Evaluation of data · Generalized least squares · ^{5}He system

1 Introduction

In astrophysics and fusion energy applications, deuteron-induced fusion reactions are important sources of energy and neutrons, and the corresponding nuclear reaction cross section is the core data for the application of this fusion reaction. Fusion cross sections are essential for designing fusion reactors [1–3] and analyzing nuclide abundance in the early universe [4, 5].

There are five types of fusion reactions currently available to us: the two reaction channels of the DD reaction, the DT reaction, the D^{3}He reaction and the TT reaction [6]. Figure 1 shows the cross sections of the five reactions. Notably, the DT cross section shows a large 5 b peak owing to the presence of the $3/2^{+}$ resonance, and the magnitudes of the DD and TT reactions are similar, being two orders of magnitude smaller than those of DT at energies below 100 keV. The D^{3}He reaction also has a peak at low energy owing to the ^{5}Li $3/2^{+}$ state (a mirror of the $A = 5$, ^{5}He state); however, because the charge of ^{3}He is larger than T, the Coulomb repulsion between D and ^{3}He is larger, so that the peak of the D^{3}He reaction cross section is lower than that of the DT reaction. As the most likely fusion reaction to be achieved, a precise study of the reaction cross section of the DT reaction is very meaningful.

Since the 1960s, it has been well established that big bang nucleosynthesis produces light elements through a series of fusion reactions. However, it is less widely recognized that the T(d,n)^{4}He reaction is responsible for producing more than 99% of the ^{4}He generated during the big bang. This ^{4}He accounts for approximately 25% (by mass) of the primordial elemental composition, with the remainder being primarily ^{1}H. The ^{4}He produced in this way serves as a crucial precursor for the triple-alpha process, which forms ^{12}C and

This work was supported by Science Challenge Project (No. TZ20180001).

✉ Tao Ye
ye_tao@iapcm.ac.cn

[1] Graduate School, China Academy of Engineering Physics, Beijing 100193, China

[2] Institute of Applied Physics and Computational Mathematics, Beijing 100094, China

[3] Department of Physics, Tsinghua University, Beijing 100084, China

subsequently enables the synthesis of heavier elements in the universe (the CNO cycle and the proton–proton chain in stars synthesize additional helium). In this sense, a portion of our human existence can be traced back to the fusion reactions.

After decades of development, many theoretical and experimental results have been accumulated [6, 7], of which the R-matrix method is an important method for nuclear data evaluation. The R-matrix theory has been primarily used in the data evaluation of light nuclear systems corresponding to fusion reactions. The introduction of R-matrix theory is aimed at theoretically describing the resonance phenomena in low-energy nuclear reactions and is mainly applied to the study of light nuclei, low-energy and nuclear reactions with distinct resonance structures. Wigner and Eisenbud were the first to propose and develop the general R-matrix theory in 1947 [8]. Starting from the Schrödinger equation of quantum mechanics, the theory uses the important concepts of atomic nucleus grouping space and channel surfaces to make the logarithmic derivatives of the wave functions of the inner and outer regions articulate on the channel surfaces, which leads to the R-matrix. By relating the R-matrix and the collision matrix, an equation can be derived that describes the cross section of the resonance phenomena in nuclear reactions.

Concerns about the current evaluation data of the ^{5}He system. Of the five major international nuclear databases, only the evaluated nuclear data file (ENDF) provides evaluation data for reaction cross sections in both neutron and deuterium channels, whereas the other databases provide evaluation data for neutron channels only. According to the ENDF file description, the current data in the ENDF database come from the R-matrix analysis of ^{5}He by Hale [9–11] and T(d,n)^{4}He Legendre coefficients evaluated by Drosg [12]. They use a multi-channel fit to data for n+^{4}He and DT reactions that extends to approximately 24 MeV excitation energy in ^{5}He system. The ENDF provides n+^{4}He data only over the original range up to 20 MeV, where single-channel scattering occurs. For the DT reaction, ENDF provides integrated cross sections and angular distributions at deuteron energies up to 10 MeV. The energy range for the T(d,n)^{4}He reaction has been extended to 30 MeV by the matching to Legendre coefficients obtained by M. Drosg. ENDF does not give errors and the covariance matrix in the evaluation data, and the comparison of the evaluation data of this work with ENDF is shown in Table 1.

At present, international R-matrix analysis programs for light nuclear data evaluation mainly include the R-matrix energy-dependent analysis code (EDA) [9], an R-matrix analysis program for light nuclear systems developed by Los Alamos National Laboratory (LANL) in the USA. We used the R-matrix Analysis Code (RAC) [13] developed by Prof. Chen Zhenpeng of Tsinghua University, which combines the generalized reduced R-matrix theory and covariance analysis theory, which has the functions of highly automated adjustment of all the R-matrix parameters and fitting a large amount of experimental data.

The RAC has two main features. First, using generalized least squares (GLS) and error propagation theory, the covariance matrix of the experimental data was used to calculate the error and covariance matrix of the accurate evaluation values.

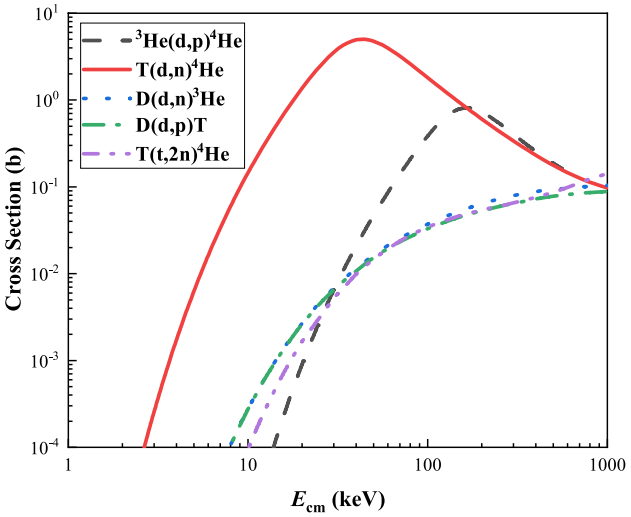

Fig. 1 (Color online) Five thermonuclear fusion cross sections versus energy in CM coordinates, data from ENDF

Table 1 Comparison of the final results of this work with ENDF/B-VIII.0, including reaction channels, energy range and whether or not to give errors

RAC			ENDF/B-VIII.0		
Reaction channel	Energy range (MeV)	Error (Y/N)	Reaction channel	Energy range (MeV)	Error (Y/N)
^{4}He(n,tot)	2.53×10^{-8}–46.0	Y	^{4}He(n,tot)	1×10^{-11}–20.0	N
^{4}He(n,el)	2.53×10^{-8}–46.0	Y	^{4}He(n,el)	1×10^{-11}–20.0	N
^{4}He(n,d)T	22.02–46.0	Y	T(d,n)^{4}He	1×10^{-4}–30.0	N
T(d,n)^{4}He	1×10^{-4}–30.0	Y	T(d,n)^{4}He*	3.71–10.0	N
T(d,n)^{4}He*	3.71–30.0	Y	T(d,el)	1×10^{-2}–10.0	N
T(d,el)	1×10^{-4}–30.0	Y			

Second, using the reduced R-matrix theory, it is possible to extend the analyzed energy region to the region of indistinguishable energy levels and to fit all available experimental data in the major energy regions. The RAC program has been used in various international collaborative projects organized by the International Atomic Energy Agency (IAEA), such as the neutron standard cross section, R-matrix program for the analysis of charged particles and International Neutron Data Evaluation Network. It has also been used to analyze the ^{12}C(n,n+3α) and ^{12}C(n,α_0)^{9}Be cross sections [14], neutron cross section standards file [15] and has obtained satisfactory results. In recent years, several efforts have been made in China to advance nuclear reaction data evaluation. Early developments, such as the UNF code for fast neutron reaction calculations [16] and the establishment of the China Evaluated Nuclear Data Library (CENDL) [17], laid an essential foundation for subsequent work [18, 19]. More recently, the continuous refinement of the CENDL−3.2 library [20] and its verification against a variety of benchmark experiments [21–23] have further strengthened China's capabilities in nuclear data evaluation. Complementary experimental studies have enriched the experimental basis for improving evaluated data libraries, including measurements of key light nucleus reactions such as ^{14}N(n,α)^{11}B [24] and ^{6}Li(n,t)^{4}He [25], as well as ^{238}U shielding benchmarks with DT neutrons [26]. The final goal is to build a complete and independent database for light nucleus reactions, covering both neutron-induced and charged-particle-induced reactions. As an indispensable component of charged-particle reactions, nuclear fusion reactions require renewed and systematic evaluations to support the development of accurate nuclear data for theoretical research and practical applications. In this study, the RAC program was used to analyze the ^{5}He system, focusing on obtaining the evaluation cross section of the neutron incident channel n+^{4}He from 2.53×10^{-8} to 46 MeV and the deuteron incident channel D+T from 1×10^{-4} to 30 MeV.

This paper provides a brief introduction to the basic reduced R-matrix theory and how to construct covariance matrices using generalized least squares. The three selected reaction channels of ^{5}He and their experimental data are discussed. The integral and differential cross sections of the T(d,n)^{4}He reactions within 0.01–0.1 MeV were analyzed. Finally, the integral cross sections and important differential cross sections for the remaining reaction channels are shown.

2 Theoretical descriptions

2.1 Generalized reduced R-matrix theory

In the generalized reduced R-matrix theory, "generalized" means that generalized least squares and "reduced" mean reduced channels. The basic R-matrix theory is described below, and the role of the reduced channels is explained. Generalized least squares is described in detail in Sect. 2.3.

The R-matrix theory is well suited for describing resonance phenomena in low-energy nuclear reactions. This allows for the adjustment of the contributions of different energy levels to each reaction channel based on experimental data, thereby achieving optimal agreement with the observations. For light nuclear systems relevant to fusion reactions, the number of resonance peaks is relatively low. In such cases, the R-matrix method can describe the cross section behavior across a wide energy range using only a few energy levels. However, the R-matrix theory has some limitations. One major issue is its inability to directly treat multi-body reaction channels. Two approaches are commonly used to address this issue in generalized reduced R-matrix theory. The first is to approximate the multi-body reaction as an effective two-body reaction. The second is to treat the multi-body channel as a reduced channel and consider only its overall contribution. This study employs the second method to handle multi-body reactions.

In 1958, Lane and Thomas explained the R-matrix theory of nuclear reactions in detail [27]. In the R-matrix approach, nuclear wave functions are described inside the channel radii by many-body basis functions, and outside the channel radii, they are described by a linear combination of two-body Coulomb functions. The reduced width amplitude is defined as the projection of the basis function to a particular channel configuration at the channel radius. This interpretation assumes that nuclear interactions occurring beyond the radius of the channel are negligible and that channels involving three or more nuclei are not essential. In addition, it is assumed that the basis functions used as Hamiltonian eigenfunctions obey a predetermined boundary constraint at the channel radius.

R-matrix theory allows the use of a set of R-matrix parameters to describe the experimental data for all two-body nuclear reactions associated with the compound nucleus. For the standard R-matrix model, the R-matrix parameters include the reduced width amplitude γ (eV$^{1/2}$), the position of the energy level E_λ (eV) and the channel radius a_c (fm). For the reduced R-matrix model, the R-matrix parameters also include the reduced channel width amplitude $\Gamma^{r}_{\lambda\mu}$ (eV), in addition to the standard R-matrix parameters, which represent the total contribution of all unconsidered reaction channels in the compound nuclear system. The advantage of considering a reduced channel width amplitude is that the R-matrix analysis can be extended to a higher-energy region.

It is assumed that a nuclear reaction system is formed after the collision between the incident particle and target nucleus. Regardless of whether the nuclear reaction system is a real compound nuclear system, the data of each reaction

channel can be fitted using the R-matrix theory. The generalized reduced R-matrix theory is then a mathematical tool that can simultaneously fit the experimental data of many types of nuclear reactions in a nuclear system. The R-matrix parameters obtained by this method are no longer required to have a clear physical meaning, as long as we can accurately describe all the experimental data. The generalized reduced R-matrix theory has been applied in the USA. R-matrix analysis program EDA and RAC were used in this work.

2.2 RAC program

Figure 2 shows the flow diagram of the RAC program. It shows the main input and output files of the RAC program and the parameter optimization process. The reliability of the R-matrix analysis results is mainly determined by the degree of conformity between the overall fitting value and the experimental data. If the fitting and experimental values are consistent within the error range, then the fitting value is reliable. The RAC program uses the GLS method to fit all the experimental data of a compound nuclear system simultaneously and finally obtains a complete set of internal self-consistent evaluation data and a covariance matrix. The formulas used to calculate the reaction cross section in the RAC program were all provided by Lane and Thomas in Chapter 10 [27].

The elements of R-matrix used in the RAC program are defined by

$$R_{c'c} = \sum_{\lambda\mu}^{N_1} \gamma_{\lambda c}\gamma_{\mu c'} A_{\lambda\mu} + \sum_{\lambda}^{N_2} \frac{\gamma_{\lambda c'}\gamma_{\lambda c}}{E_\lambda - E}, \tag{1}$$

$$\left[A^{-1}\right]_{\lambda\mu} = \left[E_\lambda^{\mathrm{res}} - E + \sum_c \left(S_c(E) - B_c\right)\gamma_{\lambda c}\gamma_{\mu c} - \frac{i}{2}\Gamma^e_{\lambda\mu}\right]\delta_{\lambda\mu}, \tag{2}$$

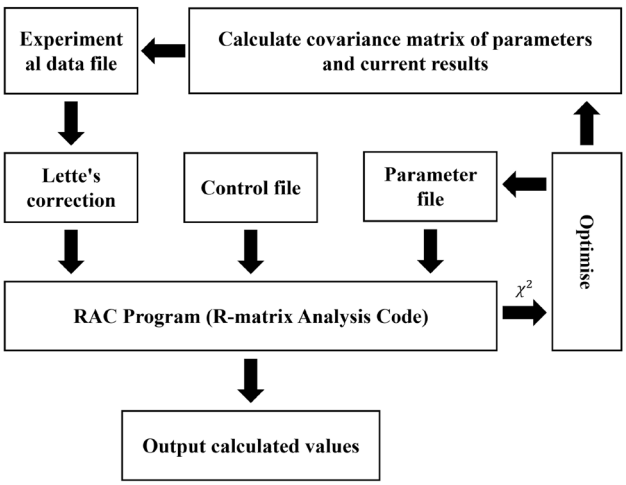

Fig. 2 (Color online) Flowchart for running the RAC program

where c and c' represent the different reaction channels. λ and μ represent the energy levels of the compound nuclear system. $\gamma_{\lambda c}$ represents the reduced width amplitude. $A_{\lambda\mu}$ represents the energy level matrix. E represents the energy in the center-of-mass system. E_λ^{res} represents the resonance energy. $S_c(E)$ represents the displacement function. B_c represents the boundary condition. $\Gamma^e_{\lambda\mu}$ represents the total reduced channel width amplitude, which is equal to the contribution of all reduced channels.

The main feature of the generalized reduced R-matrix model is the consideration of the reduced channel. In a composite nuclear system, as the energy of the composite nucleus increases, reaction channels, such as three-body and four-body reactions, will open up. However, owing to the lack of experimental data for most many-body reaction channels, it is not possible to consider them as separate reaction channels in data evaluation. Reaction channels that cannot be considered separately are categorized as reduced channels. The setup of the reduced channels can help extend the data evaluation to higher energies.

2.3 Covariances, generalized least squares and error propagation law

Smith [28] presents the professional theory for evaluation of nuclear data and is a guide to developing computer programs. Key components of nuclear data evaluation and self-contained methods are: (i) the theory of error distribution and error propagation, (ii) the formulas for covariance fitting, (iii) the theory of generalized least squares, (iv) the experimental method for modification of Pearl's pertinent puzzle (PPP), (v) Lette's criteria for minimizing the effect from occasional "outliers" (constrain the χ^2 value of "outliers," their maximum contribution is typically limited to 9), and (vi) the test for the definiteness of the covariance matrix. These components cannot be ignored if one wants to obtain an accurately evaluated value and describe the experimental nuclear data objectively and with high precision. The inherent reason for this situation stems from the fact that nuclear measurements invariably encompass long-, middle- and short-range inaccuracies in the observable factors. These inaccuracies are inevitable part of the process. A correlation was also observed between long- and middle-range errors, establishing a link between them.

In the least squares formalism, the conventional least squares (CLS) formalism is quite adequate for addressing problems in which the relationships between the observables, y, and the parameters, θ, to be estimated are inherently linear. The true values, θ_0, can never be known exactly, but our procedures aim to provide the best estimates possible for the given data. We showed that the procedure could also be used to solve nonlinear problems, provided that they are first linearized using Taylor series expansions.

This can be accomplished only if the initial estimates of the parameters, θ_a, are provided. This step within the theory is rather arbitrary. If we are in a position to make an estimate, θ_a, then we ought to be in possession of some information on its uncertainty, which should be taken into consideration in the estimation process.

The GLS formalism was introduced to rectify this deficiency in the CLS formalism. This approach represents an amalgamation of the Bayesian methodology with the least squares condition, and it is clearly the method of choice for solving nonlinear problems where the introduction of a priori estimates for the parameters is a requirement. Furthermore, the method can also be used to solve inherently linear problems that involve combining a priori information with new data to provide a refined solution. For example, we perform a Legendre fit to the differential cross-sectional data. In the first pass, estimates can be made for the Legendre expansion coefficients, α, based only on differential data. The CLS technique can be used because no prior information is available (or required). The integral information could then be introduced to derive refined values for the parameters, alpha. If the GLS is employed, all available uncertainty information will always be properly incorporated into the formalism. In fact, this approach can be used to solve problems that can be handled just as well by simpler methods. All that is required is to introduce any reasonable choice for the prior parameters, with errors sufficiently large so that the new data will be dominant.

The optimization process of the GLS method considers the full covariance matrix of the experimental data. In the GLS, both statistical and systematic errors are considered, which means that the sample no longer satisfies a strictly normal distribution, which is the actual state of our experimental dataset. There is no rigorous statistical theory that can prove that the least squares method described above can lead to the generation of an unbiased estimate. However, according to the classical statistical theory, the "Gauss–Markov" theory [28] under certain conditions, GLS can lead to the minimum variance estimation.

In the case of experimental data, the systematic error usually has great uncertainty and complexity. Some experiments yield relative measurements, some do not yield systematic errors, and some yield systematic errors that are either too large or too small. The RAC uses a repeated iterative approach to gradually replace the systematic error of the experimental data with the error of the evaluation value. To obtain the most reliable and consistent fit to the data. The analytical process of RAC requires repeated computation of the covariance matrix of the intermediate evaluated values and parameters, which involves a large amount of computation. The covariance matrix was constructed with reference to D. Smith [28].

In the following, we describe how to construct a covariance matrix with error information obtained from the experimental data. Suppose U_i^2, S_i^2, L_i^2, M_i^2 and Y_i^2 are total variance, statistical variance, long-range component (LERC) of systematic variance, medium-range (MERC) component of systematic variance and total systematic variance of i^{th} experimental data point respectively, and let $U_i^2 = S_i^2 + L_i^2 + M_i^2$, $Y_i^2 = L_i^2 + M_i^2$.

The diagonal elements C_{jj} of the correlation coefficient matrix $\mathbf{C}$ are 1 for all. The non-diagonal elements for integral cross sections are

$$C_{ij} = C_{ij}^{\mathrm{L}} + C_{ij}^{\mathrm{M}}. \tag{3}$$

Here C_{ij}^{L} refers to the LERC of systematic errors, C_{ij}^{M} refers to the MERC of systematic errors, and

$$C_{ij}^{\mathrm{L}} = \frac{L_i L_j}{U_i U_j}, \tag{4}$$

$$C_{ij}^{\mathrm{M}} = \frac{M_i M_j}{U_i U_j \cdot f_{ij}}, \tag{5}$$

$$f_{ij} = \exp\left\{-[(E_i - E_j)/W]^2/2\right\}, \tag{6}$$

where W is the distribution width parameter, and E_i and E_j are the energy points of the data.

The non-diagonal elements of $\mathbf{C}$ for differential cross section are

$$C_{ij} = (C_{ij}^{L} + C_{ij}^{M}) \cdot G_{ij}. \tag{7}$$

The correlation coefficient is determined by the total and systematic errors, and a larger systematic error leads to a larger correlation coefficient. The absolute covariance matrix elements of the simulated data can be calculated from the corresponding correlation coefficients as follows

$$V_{ij} = C_{ij} \cdot U_i \cdot U_j. \tag{8}$$

The theoretical formula for error propagation within the R-matrix model fitting is as follows

$$y - y_0 = D(P - P_0), \tag{9}$$

$$D_{ki} = (\partial y_k / \partial P_i)_0. \tag{10}$$

Here, y refers to the vector of calculated values, D is the sensitivity matrix, and P is the vector of R-matrix parameters. Subscript "0" indicates the optimized original value, and k and i are for the fitted data and R-matrix parameter subscript, respectively. The covariance matrix of parameter P is

$$V_P = (D^{+} V^{-1} D)^{-1}. \tag{11}$$

Here V refers to the covariance matrix of the data to be fitted, and its inversion matrix can be expressed as follows

$$V^{-1} = \begin{pmatrix} V_1^{-1} & & & 0 \\ & V_2^{-1} & & \\ & & \ddots & \\ 0 & & & V_k^{-1} \end{pmatrix} \tag{12}$$

where V_1, V_2 ... V_k refers to the covariance matrices of the subset data, which are independent of each other. The covariance matrix of calculated values is

$$V_y = DV_PD^+. \tag{13}$$

The formula adopted for optimizing the R-matrix fitting is

$$\begin{aligned} \chi^2 &= (\theta - \theta_P)^+ V_P^{-1}(\theta - \theta_P) \\ &+ (\eta - y)^+ V^{-1}(\eta - y) \Rightarrow \text{minimum}, \end{aligned} \tag{14}$$

where θ refers to all R-matrix parameters, V_P is the covariance matrix of the R-matrix parameters, η is the vector of experimental data, y is the vector of calculated values and V refers to the covariance matrix of the experimental data.

At the beginning of the analysis, the RAC uses χ^2 considering only the second term of Eq. (14) to fit the experimental data. After obtaining an appropriate parameter set θ and its covariance matrix V_P, the optimization formula of GLS, that is the full Eq. (14), is used to fit the experimental data. This group of θ and V_P is used as the initial values for the subsequent iteration. RAC uses an iterative process to continuously improve the estimated value of θ, and decrease the χ^2 with respect to θ and V_P simultaneously. This comes at the cost of using 100 times more CPU time than that required when using CLS or others [13]. The primary benefit of GLS is its capability to apply error propagation theory to accurately generate a covariance matrix for the evaluation data; all matrix elements of the covariance matrix are considered, whereas CLS considers only non-diagonal elements.

3 ^{5}He system analysis process

3.1 Reaction channels

Three reaction channels were considered in this study. The channel radii are listed in Table 2. The contributions of all other reaction channels are expressed in terms of the total width of the reduced channel. The initial value of channel radii a_c is given by the equation in the literature, and the equation is as follows

$$a_c = r_0(A_1^{1/3} + A_2^{1/3}), \tag{15}$$

Table 2 Channel radii of reaction channels

Reaction channel	Channel radii a_c (fm)
^{4}He + n	3.6
T + d	4.7
^{4}He* + n	5.9

where A_1 and A_2 are the mass numbers of the incident particle and target nuclei, respectively. r_0 is a constant in the range of $1.40 - 1.50$ fm. However, in the actual parameter adjustment process, the channel radii a_c is an adjustable parameter, and the final result is obtained by fitting the experimental data. The channel radii mainly influence the computation of Coulomb wave functions. By fixing the channel radii after the initial tuning, we retain the original set of Coulomb wave functions, thereby accelerating the overall optimization process.

According to the classification of incident particles, the evaluation data of the ^{5}He system were divided into the data of the neutron incident reaction channel (n+^{4}He reaction) and the data of the deuteron incident reaction channel (DT reaction). The nuclear reaction channels for neutron incident include: ^{4}He(n,tot), ^{4}He(n,el), ^{4}He(n,d)T and ^{4}He(n,np)T, and the nuclear reaction channels for deuteron incident include: T(d,n)^{4}He, T(d,el) and T(d,n)^{4}He*, where multiple reaction channels are inverse to each other. There are also deuterium capture reaction channels with very small reaction cross sections. Because both the multi-body reaction and deuterium capture cross sections are small compared to the main reaction channels for major neutron and deuterium incidences, the aforementioned reaction channels are not considered in this study.

In the calculations of R-matrix theory, the computational amount is approximately proportional to the cube of the number of reaction channels. If the incident particle energy is sufficiently high and the compound nuclear system involves many two-body and multi-body reaction channels, the number of R-matrix parameters and the computational amount can be significantly reduced using the reduced channel width amplitude. The reduced channel width amplitude is usually used to replace the contributions of two-body and multi-body reaction channels without experimental data.

In this study, the lack of experimental data on multi-body reaction channels such as ^{4}He(n,2np)D and T(d,2np)D is addressed. The contributions of these reaction channels were uniformly replaced by a reduced channel width amplitude. Based on the literature of D.R. Tilley [29], in the deuterium and tritium exit channel, the deuterium has a high probability of breaking up into a proton and a neutron. Therefore, the reaction channel ^{4}He(n,np)T was also considered in

this study. However, owing to the lack of experimental data for this reaction channel, we used the reaction T(d,n)^{4}He* with deuteron incidence in ENDF/B-VIII.0 as the inverse reaction channel for this reaction and calculated the cross section of the neutron incidence channel using the detailed balance principle in the RAC program. For ^{4}He(n,2n)^{3}He, the two-neutron emission cross section is not present in any of the evaluated nuclear data libraries or experimental data libraries, except for the special library for activation EAF-2010 [30]. The cross sections from this library were adopted; however, because the cross section of the reaction channel is extremely small, we temporarily treated its contribution as a background in the program calculations.

3.2 Use of experimental data

A more comprehensive collection of experimental data on nuclear reaction cross sections is contained in the EXFOR database [7]. This work refers to almost all the experimental data of ^{4}He+n, T+d in EXFOR. The experimental data are listed in Table 3.

When using the RAC program to optimize the R-matrix parameters based on experimental data, obvious "odd points" in the experimental data need to be excluded, and the various experimental data need to be normalized, if necessary, to prevent them from interfering with the optimization of the program and causing the R-matrix parameters to fall into erroneous positions in the high-dimensional space.

4 Analysis and discussion of results

4.1 Low energy cross section for T(d,n)^{4}He

The deuterium–tritium fusion reaction cross section is the most important reaction cross section of the ^{5}He system, dominated at low energies by a $J^{\pi} = 3/2^{+}$ resonance. This $3/2^{+}$ state increases the cross section of the DT reaction compared to other fusion reactions in the thermonuclear fusion energy region. For reactor applications, the cross-sectional data within the thermonuclear fusion energy region up to 0.1 MeV are of the greatest importance. Because the T(d,n)^{4}He reaction cross section below 0.01 MeV is extremely small, the low-energy T(d,n)^{4}He reaction cross section discussed below is mainly for 0.01–0.1 MeV. In this energy range, the T(d,n)^{4}He reaction has only experimental data for the integral cross section at its peak. There is a lack of experimental data on the differential cross section, which creates a great deal of difficulty in obtaining evaluation data, especially for the evaluation of the low-energy differential cross section.

Theoretically, the differential cross section of the T(d,n)^{4}He reaction below 0.1 MeV is very close to isotropic, and we adjusted the isotropic distribution to have a slight forward tilt and used this as an initial value. After several iterations, the initial value was replaced by the calculated value of the program, and its final calculated value was determined by fitting the entire set of experimental data. Without adding the reference data when the initial fit is in progress, it would leave too much freedom for adjusting the parameter, and it is highly possible that the low-energy differential cross-sectional data would change irregularly.

Because the R-matrix analysis for the ^{5}He system is a systematic evaluation, for the differential cross section of the T(d,n)^{4}He reaction at low energies, not only will the experimental data at that location have a constraining effect on the evaluation results, but also the experimental data in other energy ranges of the other reaction channels will have an effect on the evaluation results. In particular, the differential cross section of the neutron reaction channel ^{4}He(n,el) around 22 MeV and the differential cross-sectional data of the T(d,n)^{4}He reaction obtained only on the basis of the results of the ENDF are not objective. For the objectivity of the evaluation work, the ENDF differential cross-sectional data for low-energy T(d,n)^{4}He reaction in the original reference data were replaced using the calculated values of the current RAC program when the fitting of the full system was almost complete. According to the calculated value of the low-energy differential cross section of the T(d,n)^{4}He reaction and the experimental data of other reaction channels, the evaluation data of the differential cross section of the T(d,n)^{4}He reaction can be obtained relatively objectively in this study. Because this work is a method of covariance

Table 3 Experimental data used in the RAC program

Reaction channel	Cross-sectional type	Energy range (MeV)	Data point	Average χ^2
^{4}He(n,tot)	total cross section	1.87×10^{-7} – 40.0	167	2.89
^{4}He(n,el)	integral cross section	2.53×10^{-8} – 23.7	4	0.09
^{4}He(n,d)T	integral cross section	22.07– 22.4	11	1.81
T(d,n)^{4}He	integral cross section	7.00×10^{-3} – 16.0	238	2.67
^{4}He(n,el)	differential cross section	5.45×10^{-1} – 23.7	1098	2.59
T(d,n)^{4}He	differential cross section	1.03×10^{-2} – 20.0	929	1.46
T(d,el)	differential cross section	9.60×10^{-1} – 14.4	912	2.30

fitting, its main role is to provide the evaluation data of the error of the T(d,n)^{4}He reaction evaluation data, which is not provided by ENDF.

We finally obtained the results of the evaluation of the integral cross section and the differential cross section of the T(d,n)^{4}He reaction below 0.1 MeV, which was obtained from the existing energy level structure after a systematic evaluation of the ^{5}He system.

For the integral cross section, the current results of RAC are in good agreement with the ENDF and experimental data, and the energy region below 0.1 MeV is consistent with the ENDF results, as shown in Fig. 3. RAC-2024 and RAC-2024(2) are two different schemes in the evaluation process. The integral cross section in this energy region was used as an example to verify the conformity of the results of the two evaluation schemes and to demonstrate the accuracy of the evaluation data. RAC-2024(2) in Fig. 3 shows the results of another independent scheme that evaluated the ^{5}He system, and the results of the two schemes are basically the same, which verifies the accuracy of the evaluation data on the side. The error in the integration cross section is approximately 5‰ and the closer the energy is to the peak, the smaller the error, with an error of 2.45‰ at 0.1 MeV. The errors in the integration cross section between 0.01 MeV and 10 MeV are presented as percentages in Fig. 4. Because the T(d,n)^{4}He reaction peaks near 0.1 MeV, where the experimental data are most abundant, the error is the smallest during the error analysis. The errors in the other energy regions were larger than near 0.1 MeV, which satisfies the basic requirements of the error analysis. The covariance information is shown in Fig. 5, where we present the results of the correlation coefficients (CC) of the covariance for the integral cross section from 0.01 to 10 MeV. For the differential cross section, the results for the

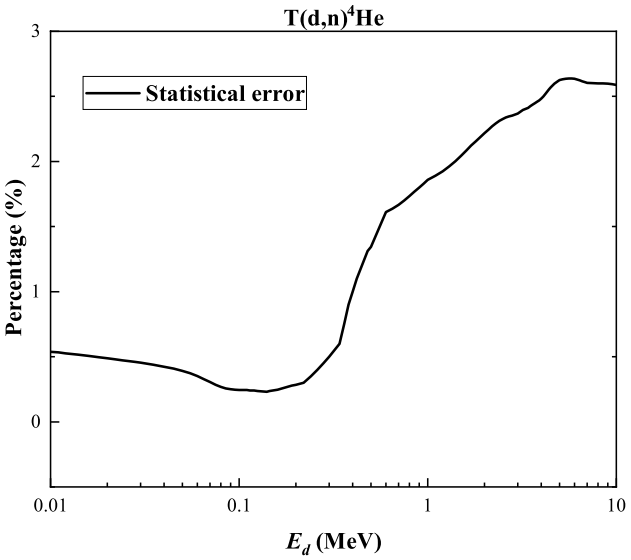

Fig. 4 Error of the T(d,n)^{4}He reaction integral cross section evaluation data given by the RAC-2024 at 0.01 to 10 MeV

differential cross section are more sensitive to the energy level structure at this position than integral cross section, and the present results differ somewhat from the ENDF. The energy level structure at this position is mainly constrained by the differential cross section for the T(d,n)^{4}He reaction below 0.1 MeV and the differential cross section of the ^{4}He(n,el) reaction at approximately 22 MeV. For the integral cross section of the T(d,n)^{4}He reaction below 0.1 MeV, the integral cross section around 22 MeV for the ^{4}He(n,el) and ^{4}He(n,tot) reactions and the interfering effects of the background play a certain role.

Figure 6 shows the results of the evaluation of differential cross sections at 0.01, 0.05 and 0.09 MeV. As can be seen from these figures, the center values of the RAC evaluation

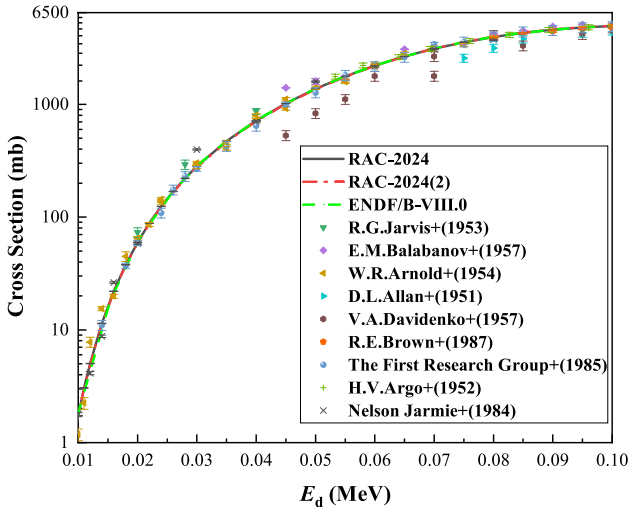

Fig. 3 (Color online) T(d,n)^{4}He from 0.01 to 0.1 MeV

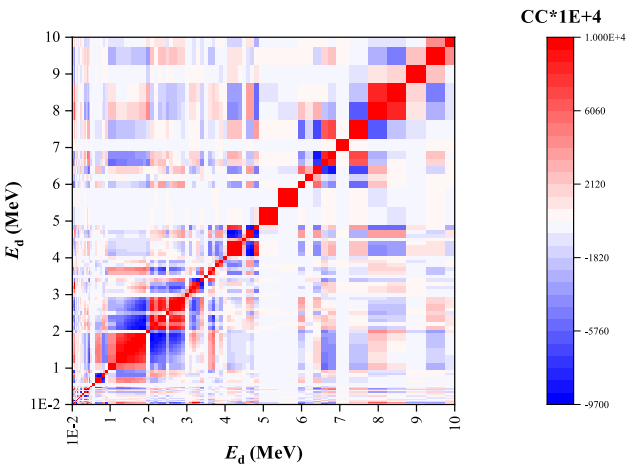

Fig. 5 (Color online) Correlation coefficients (multiply by 1×10^4) of the covariance for T(d,n)^{4}He from 0.01 to 10 MeV

results are somewhat different from the ENDF results, with the difference in center values being within 5‰ and the ENDF results are within the error range of the RAC evaluation results. The differential cross section of the T(d,n)^{4}He reaction at low energy tends to be essentially isotropic. Detailed differential cross-sectional data on the results of the RAC evaluation can be found in the supplementary file (pages 6-19).

Here is an individual discussion of the differential cross section at $E_d = 0.1$ MeV and a discussion of why the low-energy differential cross section is forward-sloping from the point of view of wave splitting. $E_d = 0.1$ MeV is basically where the peak is, and it is very important to determine how the differential cross section of 0.1 MeV is constructed. The contributions of the different energy levels at the peak are analyzed in the following section. As the analysis of the $A = 5$ systems progresses, an accurate knowledge of the reaction channel T(d,n)^{4}He is expected to contribute to our knowledge of the levels of ^{5}He. The resonance observed at a low energy of $E_d = 109$ keV is widely recognized to be attributable to the $J^\pi = 3/2^+$ state in ^{5}He.

In the present study, the angular distribution at the peak $E_d = 0.1$ MeV is forward-sloping, and the following explains the cause of the forward lean tendency of the angular distribution at the peak. The angular distribution is energy level dependent. We used Legendre polynomials to decompose the angular distribution at 0.1 MeV. Each Legendre polynomial coefficient reflects the contribution of a specific energy level with different orders corresponding to different physical effects. The formula used to calculate the angular distribution is shown below

$$p_i(\mu, E) = \frac{1}{2} + \sum_{l=1}^{NL} \frac{2l+1}{2} a_l(E) P_l(\mu), \tag{16}$$

where P_l is a Legendre polynomial with a maximum order of NL. Note that the angular distribution p_i is normalized by the integral cross section. Only the first four terms of the Legendre polynomial were considered, with a_0 defaulting to 1. The other coefficients are listed in Table 4 (for higher-order fits, see the supplementary file on pages 4-5). The Legendre polynomials were calculated as shown in Fig. 7.

Decomposing Legendre polynomials for the angular distribution, different l have different shapes. For example, the S-wave, l=0, is horizontal, and no extremes occur. The P-wave, l=1, shows a tendency to be a straight line with a high left and low right. The D-wave, l=2, is extremely large at 0° and 180° and extremely small at 90°. Table 4 and Fig. 7 show that the value of a_1 is much larger than that of a_2 and a_3, and that the S-wave together with the small contribution of the P-wave has basically constituted the shape of the angular distribution of the forward tendency. From the R-matrix energy level parameters, the P-wave at this position mainly originated from the $3/2^-$.

This problem can also be analyzed in terms of the wave splitting contribution. All waves were discussed separately, and for each wave, their contribution to the angular distribution at that energy was calculated individually, and the results are shown in Fig. 8. As shown, $J^\pi = 3/2^+$ makes

Table 4 Legendre coefficients for differential cross sections at 0.01, 0.05 and 0.1 MeV for T(d,n)^{4}He reaction

E_d (MeV)	CS (mb)	a_1	a_2	a_3
0.01	1.732×10^{0}	2.808×10^{-4}	2.203×10^{-4}	4.312×10^{-6}
0.05	1.370×10^{3}	4.614×10^{-4}	1.688×10^{-4}	-4.429×10^{-6}
0.1	4.936×10^{3}	1.342×10^{-3}	-1.849×10^{-4}	-3.599×10^{-6}

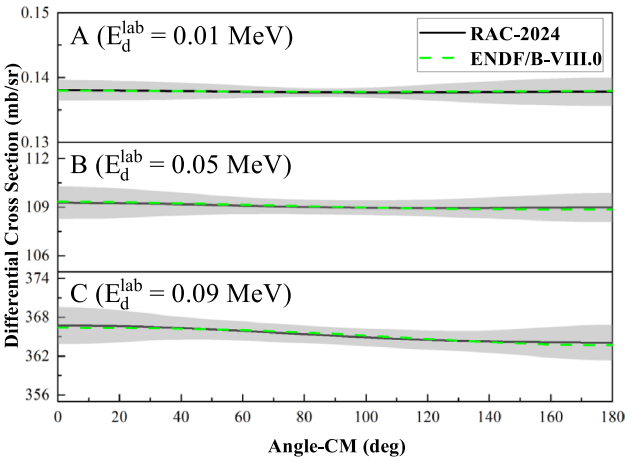

Fig. 6 (Color online) Differential cross section at 0.01, 0.05 and 0.09 MeV for the T(d,n)^{4}He reaction

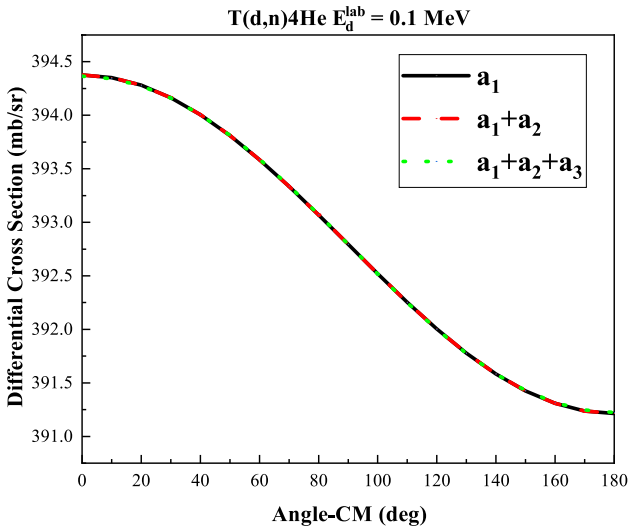

Fig. 7 (Color online) Calculations of Legendre functions of different orders for the T(d,n)^{4}He angular distribution at 0.1 MeV

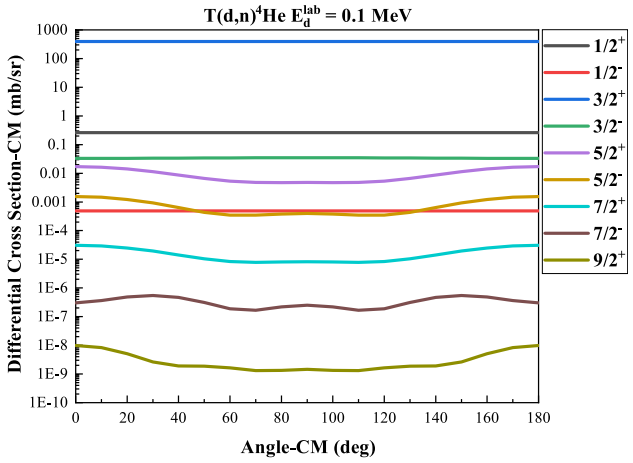

Fig. 8 (Color online) Independent contributions of each wave to the T(d,n)^{4}He angular distribution at 0.1 MeV in center-of-mass systems

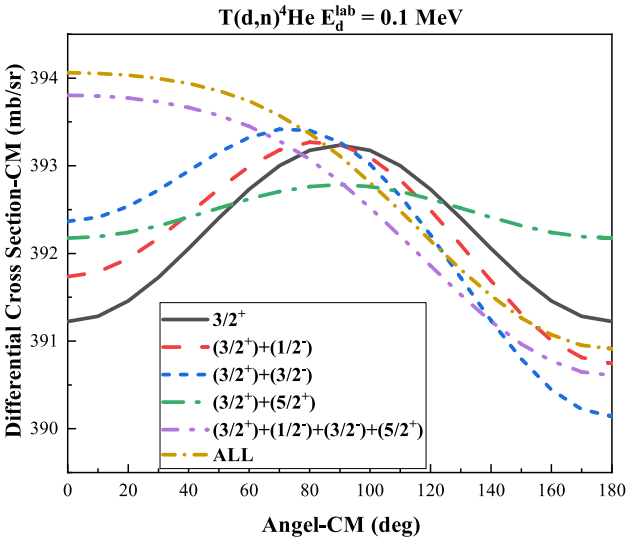

Fig. 9 (Color online) Contributions of the four waves $1/2^-$, $3/2^+$, $3/2^-$ and $5/2^+$ versus the final result in center-of-mass systems

the main contribution to the angular distribution at that energy point, and the contributions of the other waves are significantly smaller than the contribution of $J^\pi = 3/2^+$. However, the contributions of individual waves are almost all 90° symmetric, which cannot explain the phenomenon of angular distribution leaning forward, from which it can be recognized that the angular distribution leaning forward should be formed due to the interference between individual waves. The angular distribution of $J^\pi = 3/2^+$ at 0.1 MeV is a raised peak, and $J^\pi = 3/2^+$ interferes with $J^\pi = 1/2^-$ and $J^\pi = 3/2^-$, making the calculated values of the angular distribution larger at small angles and smaller at large angles. The magnitude of the interference for $J^\pi = 3/2^+$ with $J^\pi = 3/2^-$ is larger than that for $J^\pi = 1/2^-$. The interference between $J^\pi = 3/2^+$ and $J^\pi = 5/2^+$ depresses the peak of the angular distribution results for $J^\pi = 3/2^+$ and improves the results for large and small angles. In summary, the four waves $J^\pi = 1/2^-$, $J^\pi = 3/2^+$, $J^\pi = 3/2^-$ and $J^\pi = 5/2^+$ then essentially compose the angular distribution of 0.1 MeV, and the result is shown in Fig. 9.

4.2 Other reaction cross sections of the ^{5}He system

Owing to the excessive amount of data for the evaluation of the ^{5}He system, this section only shows and illustrates the integral cross sections and individual differential cross sections considered in this work. For detailed information, refer to the supplementary file (including integral cross sections, differential cross sections and neutron polarization differential cross sections).

Figures 10 and 11 show the comparison of the results of all integral cross sections in this study with the experimental and evaluation data. For neutron incidence channels, ENDF/B-VIII.0 provides evaluation data up to 20 MeV, except for ^{4}He(n,d)T. For the deuterium incidence channel, ENDF/B-VIII.0 provides evaluation data up to 30 MeV. The results of this study are generally consistent with ENDF/B-VIII.0 within the energy range considered by the ENDF file. The ENDF data referenced later were obtained from ENDF/B-VIII.0.

It should be mentioned that for the total neutron incident cross section, the present work extends the incident neutron energy up to 46 MeV. As shown in Figs. 10a and 11, especially at the second peak caused by the energy level of $3/2^+$ owing to T(d,n)^{4}He opening at approximately 22 MeV, the RAC results are consistent with the experimental data within the error range. According to Tilley [29], this energy level corresponds to the first $3/2^+$ state in the compound nuclear system of ^{5}He. This indirectly indicates that the level distribution obtained within the RAC framework is generally consistent with the experimentally measured level distribution. Here, the experimental data have large errors; therefore, it is not a strong constraint for the optimization of the R-matrix parameters. The level distribution in this energy region is mainly constrained by the experimental data of the integral and differential cross sections near the first peak of the T(d,n)^{4}He reaction as well as the differential cross sections of the ^{4}He(n,el) reaction in the same energy range. Compared to the integrated cross sections, the differential data provide stronger constraints, as the differences in the shape of the differential cross sections directly determine which partial waves are involved at a given energy.

The elastic scattering cross section for neutrons is shown in Fig. 10b. Because the other reaction channels of the ^{5}He system are not yet open before 20 MeV, the neutron elastic scattering cross section is completely consistent with the total neutron cross section in this energy range. This reaction

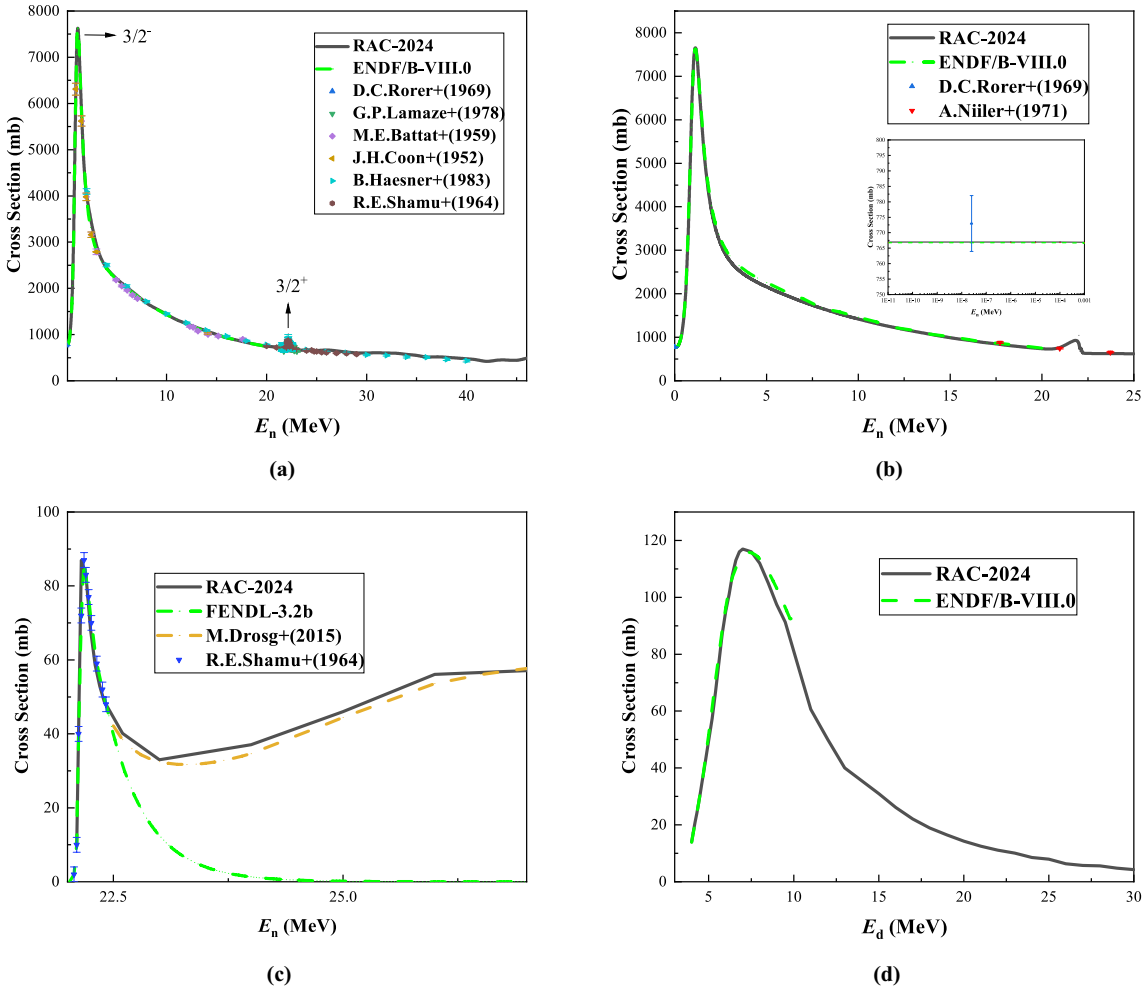

Fig. 10 (Color online) Evaluation data of the integral cross sections for other reaction channels of the ^{5}He system. **a** ^{4}He(n,tot) from 1×10^{-11} to 46 MeV; **b** ^{4}He(n,el) from 1×10^{-11} to 25 MeV in linear coordinate. The micrograph shows results from 1×10^{-11} to 1×10^{-3} MeV in log–log coordinates; **c** ^{4}He(n,d)T from 22 to 27 MeV; **d** T(d,n)^{4}He* from 3.5 to 30 MeV. ^{4}He* is the first excited state of ^{4}He

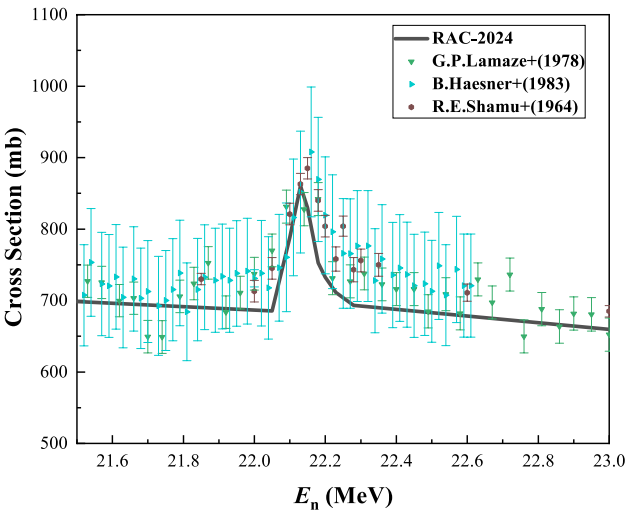

Fig. 11 (Color online) ^{4}He(n,tot) from 21.5 to 23 MeV

cross section shows a small peak at approximately 22 MeV, as does the total cross section, which again is the contribution of the 3/2^{+} energy level at this energy. The experimental data for neutron elastic scattering have only four energy points, at thermal energy and near 20 MeV, and the results of the RAC are consistent with both the ENDF evaluation data and the experimental data within the error range.

The deuteron emission cross section for the neutrons is shown in Fig. 10c. The deuteron emission cross section has a threshold of 22.02 MeV, and only Shamu [31, 32] measured the cross section at the first peak at 22.2 MeV. The FENDL-3 library references these experimental data, and the FENDL-3 library requirement is for all evaluation data to be at least 60 MeV, extrapolating the cross section to 60 MeV by following the trend of the last four measured points on a log–log scale. The extrapolated data were published in the FENDL-3.2b. Drosg [12] has also calculated the results for this reaction channel by detailed balance

calculations. A comparison of the RAC with FENDL-3.2b, Drosg's data and the experimental data is shown in Fig. 10c. There is a lack of experimental data after the first peak, and because this work is a systematic evaluation of ^{5}He system, the region lacking experimental data follows the cross section of the inverse reaction T(d,n)^{4}He. This is the reason why the RAC results are consistent with Drosg's results. Following the principle of detailed balance, after the first peak of this reaction, the cross section rises gradually as the energy increases and does not decrease.

Figure 10d shows the reaction cross section of T(d,n)^{4}He* where ^{4}He* refers to the first excited state of ^{4}He. The RAC and ENDF results were generally in agreement. We extrapolated the cross tion for this reaction based on the R-matrix parameters of the present work to a maximum energy of 30 MeV.

The differential cross section of each reaction channel was consistent with the experimental data. It should be mentioned that the differential cross section of neutron elastic scattering around 22 MeV plays a very important role in constraining the low-energy differential cross section of the T(d,n)^{4}He reaction. Figure 12a shows a comparison of the RAC at 21.85 MeV with the experimental data.

It should be noted that, for the T(d,el) reaction, we used experimental data that were not included in the ENDF evaluation. The RAC results showed good agreement with the experimental data. Figure 12b shows the results of the evaluation of the RAC at 13.85 MeV in comparison with the new experimental data [33].

5 Summary

In this study, based on the generalized reduced R-matrix theory, the RAC program was used to simultaneously calculate and analyze all available experimental data on the ^{5}He system. The evaluation values of the main reaction cross sections of the ^{5}He system were obtained after setting reasonable reaction channels, gradually adding and adjusting suitable R-matrix energy levels, and repeatedly iterating and adjusting the R-matrix parameters. Compared with the existing mainstream evaluation database, the overall conformity was good, and the errors were within the allowable range. Simultaneously, we combined physical principles or mathematical methods to obtain valid data that could be added to the analysis, expanding the data sources and improving the credibility of the calculated values. In particular, the error and covariance matrix of the T(d,n)^{4}He reaction cross section evaluation are provided for the first time.

For the integral cross section, the maximum energy of neutron incidence is generally widened to 46 MeV, and the maximum energy of deuterium incidence is generally widened to 30 MeV, which enlarges the scope of the evaluation data. For the differential cross section, the results are given for the four reaction channels ^{4}He(n,el), ^{4}He(n,d)T, T(d,n)^{4}He and T(d,el) at different incidence energies, which is very broad and basically covers the range of the existing experimental data. In particular, the low-energy differential cross section for the T(d,n)^{4}He reaction was analyzed in detail, and wave splitting analysis of the angular distribution at 0.1 MeV was performed using Legendre polynomials. The

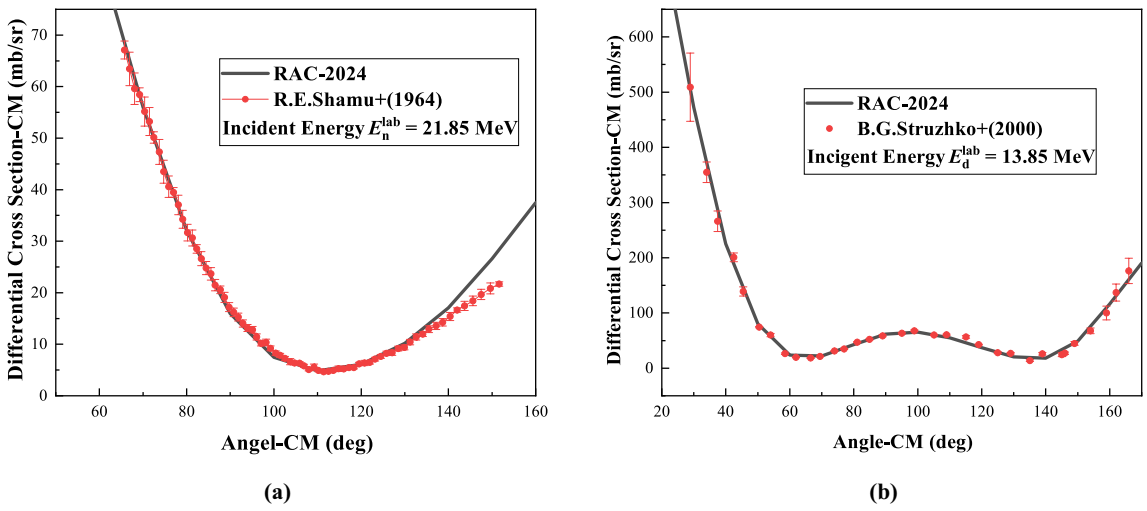

Fig. 12 Evaluation data of the integral cross sections for other reaction channels of the ^{5}He system. **a** Differential cross section of the ^{4}He(n,el) at 21.85 MeV; **b** Differential cross section of the T(d,el) at 13.85 MeV

reason for the forward slope of the differential cross section near the peak is given in terms of the contribution of the S-wave and P-wave from $3/2^{-}$. For error analysis, the errors in the integral and differential cross sections of each reaction channel, as well as the covariance of the integral cross sections, were calculated using the generalized least squares and error propagation theories. In the evaluation data of several reciprocal reactions in the ^{5}He system, the cross-sectional data were precisely matched, which further ensured the reliability of the final evaluation data.

Supplementary Information The online version contains supplementary material available at https://doi.org/10.1007/s41365-025-01874-2.

Acknowledgements We thank the other members of the Nuclear Physics Faculty at the Institute of Applied Physics and Computational Mathematics for their assistance with this study.

Author Contributions All authors contributed to the study conception and design. Material preparation, data collection and analysis were performed by XH, TY and Z-PC. The first draft of the manuscript was written by XH and all authors commented on previous versions of the manuscript. All authors read and approved the final manuscript.

Data Availability The data that support the findings of this study are openly available in Science Data Bank at https://cstr.cn/31253.11.sciencedb.j00186.00813 and https://www.doi.org/10.57760/sciencedb.j00186.00813.

Declarations

Conflict of interest The authors declare that they have no conflict of interest.

References

1. J. Ongena, Y. Ogawa, Nuclear fusion: status report and future prospects. Energy Policy **96**, 770–778 (2016). https://doi.org/10.1016/j.enpol.2016.05.037
2. X.Z. Li, B. Liu, S. Chen et al., Fusion cross-sections for inertial fusion energy. Laser Part. Beams **22**, 469–477 (2004). https://doi.org/10.1017/S026303460404011X
3. X.Z. Li, Q.M. Wei, B. Liu et al., A new simple formula for fusion cross-sections of light nuclei. Nucl. Fusion **48**, 125003 (2008). https://doi.org/10.1088/0029-5515/48/12/125003
4. W.F. Li, N. Wang, F. Jia et al., Particle transfer and fusion cross-section for super-heavy nuclei in dinuclear system. Nucl. Part. Phys. **32**, 1143 (2006). https://doi.org/10.1088/0029-5515/48/12/125003
5. C.L. Jiang, K.E. Rehm, B.B. Back et al., Expectations for ^{12}C and ^{16}O induced fusion cross sections at energies of astrophysical interest. Phys. Rev. C **75**, 015803 (2007). https://doi.org/10.1103/PhysRevC.75.015803
6. M.B. Chadwick, M.W. Paris, G.M. Hale et al., Early nuclear fusion cross-section advances 1934–1952 and comparison to Today's ENDF data. Fusion Sci. Technol. (2024). https://doi.org/10.1080/15361055.2023.2297128
7. V.V. Zerkin, B. Pritychenko, The experimental nuclear reaction data (EXFOR): extended computer database and web retrieval system. Nucl. Instrum. Meth. A **888**, 31–43 (2018). https://doi.org/10.1016/j.nima.2018.01.045
8. E.P. Wigner, L. Eisenbud, Higher angular momenta and long range interaction in resonance reactions. Phys. Rev. **72**, 29–41 (1947). https://doi.org/10.1103/PhysRev.72.29
9. G.M. Hale, M.W. Paris, Data covariances from R-Matrix analyses of light nuclei. Nucl. Data Sheets **123**, 165–170 (2015). https://doi.org/10.1016/j.nds.2014.12.029
10. G.M. Hale, T.L. Talley, Deuteron-induced fusion in various environments, in *Proc. of the Inter. Conf. on Nuclear Data for Science and Technology* (1994), 102493181
11. G.M. Hale, T.L. Talley, Cross sections and spectra for charged-particle induced reactions, in *Proc. of the Inter. Conf. on Nuclear Data for Science and Technology* (1994). 11197868
12. M. Drosg, DROSG-2000: Neutron source reactions. Data files with computer codes for 56 monoenergetic neutron source reactions. IAEA (2000). IAEA-NDS-87(rev.5)
13. Z.P. Chen, Y.Y. Sun, A global fitting method with the R-matrix code RAC. IAEA (2019). https://doi.org/10.61092/iaea.zr3b-121v
14. J. Liu, Z.Q. Cui, Y.W. Hu et al., ^{12}C(n, n+3α) and ^{12}C(n,α_0)^{9}Be cross sections in the MeV neutron energy region. Phys. Lett. B **842**, 137985 (2023). https://doi.org/10.1016/j.physletb.2023.137985
15. V.G. Pronyaev, S.A. Badikov, Z.P. Chen et al., Status of the international neutron cross-section standards file. AIP Conf. Proc. **769**, 808–815 (2005). https://doi.org/10.1063/1.1945130
16. J.S. Zhang, UNF code for fast neutron reaction data calculation. Nucl. Sci. Eng. **142**, 207–219 (2002). https://doi.org/10.13182/NSE02-02
17. D.J. Cai, Q.C. Liang, T.J. Liu et al., Chinese evaluated nuclear data library, version 2 (CENDL-2). Chin. J. Nucl. Sci. Eng. **17**, 257–265 (1997). https://doi.org/10.1007/978-3-642-58113-7_225 **(Color online)**
18. Z.G. Ge, R.R. Xu, P. Liu, Nuclear data evaluation and Chinese evaluated nuclear data library. Atom. Energy Sci. Technol. **56**, 783–797 (2022). https://doi.org/10.7538/yzk.2022.youxian.0221
19. T.J. Zu, Y.H. Huang, Q.C. Teng et al., Application of CENDL-3.2 and ENDF/B-VIII.0 on the reactor physics simulation of PWR. Ann. Nucl. Energ. **158**, 108238 (2021). https://doi.org/10.1016/j.anucene.2021.108238
20. Z.G. Ge, R.R. Xu, H.C. Wu et al., CENDL-3.2: the new version of Chinese general purpose evaluated nuclear data library. EPJ Web Conf. **239**, 09001 (2020). https://doi.org/10.1051/epjconf/202023909001
21. W.Y. Shu, T.J. Zu, L.Z. Cao et al., Performance of CENDL-3.2 evaluated nuclear data library for the shielding benchmarks. Prog. Nucl. Energ. **136**, 103727 (2021). https://doi.org/10.1016/j.pnucene.2021.103727
22. J.J. Hu, B. Zhang, Z.W. Zong et al., Verification of CENDL-3.2 nuclear data on VENUS-3 shielding benchmark by ARES transport code. Sci. Technol. Nucl. Ins. **3**, 1–13 (2021). https://doi.org/10.1155/2021/6633366
23. T.Y. Huang, Z.G. Li, S.H. Jiang et al., Verification of CENDL-3.2 and ENDF/B-VIII.0 evaluated nuclear data library on HTR-10 benchmark. Front. Energ. Res. **9**, 829402 (2022). https://doi.org/10.3389/fenrg.2021.829402
24. Y.W. Hu, Y.M. Gledenov, Z.Q. Cui et al., Cross section measurement for the ^{14}N(n,α0,1)^{11}B reactions in the 4.5–11.5 MeV neutron energy region. Eur. Phys. J. A **60**, 51 (2024). https://doi.org/10.1140/epja/s10050-024-01268-9
25. G.H. Zhang, J.X. Chen, G.Y. Tang et al., Measurement of differential and angle-integrated cross sections of the ^{6}Li(n, t)^{4}He reaction in the MeV neutron energy range. Nucl. Instrum. Meth. A **566**, 615–621 (2006). https://doi.org/10.1016/j.nima.2006.06.064

26. Y.Y. Ding, Y.B. Nie, Y. Zhang et al., Benchmark experiment on slab ^{238}U with D-T neutrons for validation of evaluated nuclear data. Nucl. Sci. Tech. **35**, 29 (2024). https://doi.org/10.1007/s41365-024-01386-5
27. A.M. Lane, R.G. Thomas, R-matrix theory of nuclear reactions. Rev. Mod. Phys. **30**, 257–353 (1958). https://doi.org/10.1103/RevModPhys.30.257
28. D.L. Smith, *Probability, statistics, and data uncertainties in nuclear science and technology*. American Nuclear Society (1991). ISBN: 0-89448-036-7
29. D.R. Tilley, C.M. Cheves, J.L. Godwin, Energy levels of light nuclei $A = 5, 6, 7$. Nucl. Phys. A **708**, 3–163 (2002). https://doi.org/10.1016/S0375-9474(02)00597-3
30. L.W. Packer, The European activation file: EAF-2010 biological, clearance and transport libraries. CCFE (2010), 61380664
31. R.E. Shamu, J.G. Jenkin, Neutron-alpha scattering in the 20-MeV range. Phys. Rev. **135**, B99 (1964). https://doi.org/10.1103/PhysRev.135.B99
32. R.E. Shamu, G.G. Ohlsen, P.G. Young, The He^5 states at high excitation energies. Phys. Lett. **4**, 286–288 (1963). https://doi.org/10.1016/0031-9163(63)90603-6
33. B.G. Struzhko, Angular distribution of nucleon pairs in d + t reaction at the deutron energy of 13.85 MeV. Bull. Russ. Acad. Sci. Phys. **64**, 370 (2000)